Proceedings of
2001 ASME International Mechanical Engineering Congress and Exposition
November 11-16, 2001, New York, NY

IMECE2001/MEMS-23924

DESIGN AND EXPERIMENTAL RESULTS OF SMALL-SCALE ROTARY ENGINES

Kelvin Fu, Aaron J. Knobloch, Fabian C. Martinez, David C. Walther, Carlos Fernandez-Pello*, Al P. Pisano, Dorian Liepmann
University of California at Berkeley
Berkeley, CA 94720
Phone: 510-642-6554, Fax: 510-642-6163
Email:ferpello@me.berkeley.edu

Kenji Miyaska
Department of Technology
Fukui University
Fukui, Japan

Kaoru Maruta
Department of Machine Intelligence and Systems Engineering
Faculty of Systems Science and Technology
Akita Prefectural University, Japan

ABSTRACT

A research project is currently underway to develop small-scale internal combustion engines fueled by liquid hydrocarbons. The ultimate goal of the MEMS Rotary Internal Combustion Engine Project is to develop a liquid hydrocarbon fueled MEMS-size rotary internal combustion micro-engine capable of delivering power on the order of milli-watts. This research is part of a larger effort to develop a portable, autonomous power generation system with an order of magnitude improvement in energy density over alkaline or lithium-ion batteries. The rotary (Wankel-type) engine is well suited for the fabrication techniques developed in the integrated chip (IC) community and refined by the MicroElectroMechanical Systems (MEMS) field. Features of the rotary engine that lend itself to MEMS fabrication are its planar construction, high specific power, and self-valving operation.

The project aims at developing a "micro-rotary" engine with an epitrochoidal-shaped housing under 1 mm^3 in size and with a rotor swept volume of 0.08 mm^3. To investigate engine behavior and design issues, larger-scale "mini-rotary" engines have been fabricated from steel. Mini-rotary engine chambers are approximately 1000 mm^3 to 1700 mm^3 in size and their displacements range from 78 mm^3 to 348 mm^3.

A test bench for the mini-rotary engine has been developed and experiments have been conducted with gaseous-fueled mini-rotary engines to examine the effects of sealing, ignition, design, and thermal management on efficiency. Preliminary testing has shown net power output of up to 2.7 W at 9300 RPM. Testing has been performed using hydrogen-air mixtures and a range of spark and glow plug designs as the ignition source. Iterative design and testing of the mini-engine has lead to improved sealing designs. These particular designs are such that they can be incorporated into the fabrication of the micro-engine.

Design and fabrication of a first generation meso-scale rotary engine has been completed using a SiC molding process developed at Case Western Reserve University. The fabrication of the micro-rotary engine is being conducted in U.C. Berkeley's Microfabrication Laboratory.

Testing of the mini-engine has lead to the conclusion that there are no fundamental phenomena that would prevent the operation of the micro-engine. However, heat loss and sealing issues are key for efficient operation of the micro-engine, and they must be taken into account in the design and fabrication of the micro-rotary engine. The mini-rotary engine design, testing, results and applications will be discussed in this paper.

NOMENCLATURE

Bi	Biot Number
e	Engine Eccentricity
h	Convection Coefficient
k	Ratio of Specific Heats
k_{solid}	Conduction Coefficient
l	Length
n_E	Output Shaft Speed
r_v	Compression Ratio
r_c	Cutoff Ratio
R	Rotor Generating Radius
t_{res}	Residence Time
t_{chem}	Chemical Time
T_m	Temperature (Melting)
u	Velocity
V_s	Swept Volume (Displacement)
w	Engine Width
ε_{th}	Theoretical Compression Ratio
Φ	Equivalence Ratio
η_{th}	Thermal Efficiency

INTRODUCTION

MicroElectroMechanical Systems (MEMS) devices are mechanical elements constructed using the manufacturing techniques and materials used in the integrated circuit / microchip industry [1,2]. Typically, MEMS fabrication uses lithography to mask the silicon substrate, followed by etching and deposition to create the high aspect ratio features in the substrates. The combination of small scale and potentially inexpensive mass production is the primary attraction of the technology. Early products in the MEMS field (accelerometers and gyroscopes) have given way to other, more complex, engineering systems (head-mounted displays, optical communication systems, and micro-fluidic systems). As new manufacturing techniques and materials have been developed, MEMS-scale thermal devices are now practical [3]. These microscale engines have numerous applications, because the power output can be electrical or mechanical (torque). Applications range from mobile electrical power supplies (potential battery replacements) to mechanical power.

The ultimate goal of the MEMS Rotary Internal Combustion Engine Project is to fabricate a micro-rotary 'Wankel' engine, which produces ~10-100 mW of mechanical power. The engine chamber will fit in a cubic millimeter, with a swept volume of 0.08 mm^3. A power generation system using the micro-rotary engine would have 5 times to 14 times the energy density of a primary battery [4] (see Fig. 1). The MEMS scale "micro-rotary" engine will be constructed primarily of Silicon (Si), Silicon Carbide (SiC), and Silicon Dioxide (SiO_2). All parts subjected to high temperatures and stresses will be built either using molded SiC [5] or a Si substrate with a thin SiC coating [6].

The research program is planned in progressive steps leading to the fabrication of a MEMS-scale engine. A series of larger scale "mini-rotary" engines, with swept volumes of 78 mm^3 to 348 mm^3, have been constructed to investigate design and combustion issues as the engine scale is reduced. In addition, fabrication of the microrotary engine has begun. This paper describes the challenges of building a small-scale rotary engine from testing, design, and MEMS fabrication viewpoints and suggests solutions to these challenges.

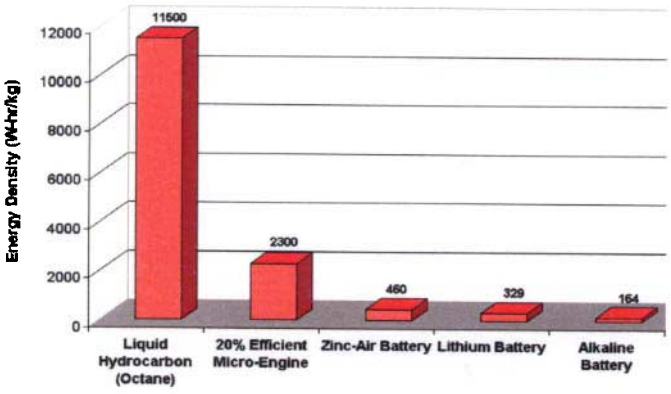

Figure 1. Comparison of energy densities between internal combustion engines and primary batteries.

ROTARY ENGINE LAYOUT AND DESIGN

A rotary engine was selected for development as the basis of a MEMS-scale power generation system due to several factors:

- the planar design of the rotary engine lends itself to MEMS fabrication
- the rotor controls the timing of the intake and exhaust, eliminating the need for the complex valve actuating and valve timing systems found in 4-stroke reciprocating engines
- the power output is in the form of rotary motion of the shaft, which is necessary for powering either a micro-vehicle or an electric generator

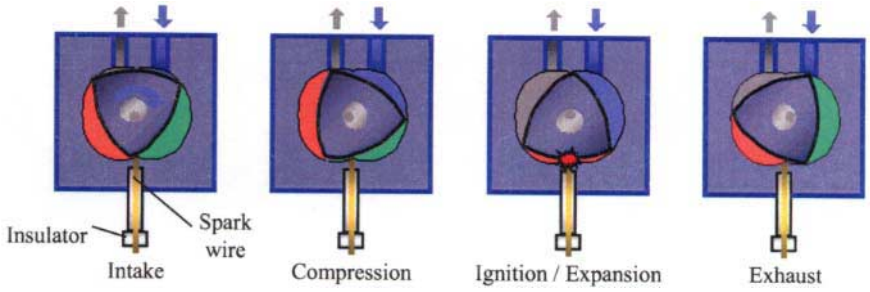

Figure 2. Rotary Engine Operation

The rotary engine consists of a triangular rotor rotating within an epitrochoidal-shaped housing (see Fig. 2). The rotor centerline is offset from the housing centerline by an eccentric, *e*. As the rotor rotates about the center of the epitrochoid, all three apexes of the rotor remain in contact with the walls, forming three sealed chambers. In large-scale systems, an elaborate sealing system is used to prevent leakage: 1) over the face of the rotor (face seals) and 2) around the rotor ends (apex seals). The seals incorporated into the present work will be addressed later in this paper.

The rotary engine operates on a 4-stroke cycle, as illustrated in Figure 2. As the rotor apex passes over the intake port, the increasing volume in the chamber draws in a fresh fuel / air charge (intake). The rotor continues to rotate, and the next apex closes the intake port and compresses the fuel / air mixture (compression). The fuel / air mixture is ignited using a spark plug, glow plug, or compression ignition. The resulting pressure rise acts off the rotor axis due to the eccentricity, *e*, leading to a torque from which the shaft work is extracted (power). After the power stroke, the rotor apex uncovers the exhaust port. As the rotor continues to rotate, the exhaust gases are ejected from the engine by the decreasing volume (exhaust). The rotor apex then uncovers the intake port again, taking in a fresh charge. Since there are three chambers formed by the rotor and epitrochoid, this cycle occurs three times for every revolution of the rotor. The rotor spins at 1/3 the speed of the output shaft, resulting in one power pulse for every revolution of the shaft. References to engine speed in this paper

Table 1. Mini-Engine Characteristics

	MN125	MN50	MN30
Estimated Power (W)	125	50	30
Operating Speed (RPM)	30,000	30,000	30,000
Displacement (mm^3)	348	138	78
Liq. Fuel Consumption (ml/sec)	0.017	0.0068	0.0039
CO_2 Output (mL/sec)	35	14	8
Heat Output (W)	486	193	109
Rotor Diameter (mm)	12.6	12.3	9.4
Width (mm)	9.0	3.5	3.6

refer to the output shaft rotational speed.

The three primary engine parameters are: the rotor generating radius (R), the rotor width (w), and the eccentricity (e). Once these are established, all other engine parameters (displacement, theoretical compression ratio, maximum tip velocity, and tip angle) are also established [7,8]. Table 1 gives basic engine data for several mini-engines developed for different potential applications.

Table 2. Basic Rotary Engine Parameter Calculations

Parameter	Equation
Displacement [7]	$V_s = 3\sqrt{3}Rwe$
Theoretical Compression Ratio [8]	$\varepsilon_{th} = 1 + \dfrac{9\sqrt{3}eR}{e^2\pi + eR\left(8\cos\phi - 3\sqrt{3}\right) + \phi\left(\dfrac{2R^2}{3} + 12e^2\right)}$ where $\sin\phi = \dfrac{3e}{R}$
Maximum Tip Velocity [8]	$u_{\max} = \dfrac{2\pi n_E\left(\dfrac{R}{3} + e\right)}{1000}$ where n_E = output shaft speed (rev/s)

Table 2 lists the basic equations [7,8] used to calculate rotary engine parameters. Some notes concerning the compression ratio should be made. High compression ratio in rotary engines requires a low R/e ratio, which means a small rotor radius and high eccentricity. For instance, an R/e ratio of 11.5 gives a theoretical compression ratio of 30:1. However, the higher R/e ratio also results in a higher maximum tip angle (the angle at which the rotor apex is in contact with the epitrochoid chamber) and higher surface to volume ratio at maximum compression. The higher tip angle is detrimental to sealing effectiveness, as well as seal durability [8]. The higher surface to volume ratio in the combustion chamber will accelerate heat loss. Therefore, every rotary engine design is a compromise between sealing effectiveness, surface to volume ratio, and compression ratio. The mini engines have a R/e ratio of approximately 7.

The compression ratio in a working rotary engine is also never as high as the theoretical compression ratio. All rotary engines have a rotor cutout to allow the combustion reaction to propagate at the onset of the power stroke. The theoretical compression ratio does not take the rotor cutout into account, because the cutouts are different for each engine.

A series of mini-rotary engines of intermediate size (78 mm^3 to 348 mm^3) have been built and used to study combustion, fluid, and design issues as the engine is reduced in size. The design of the mini-rotary mimics the proposed design of the micro-rotary. Each engine has different power outputs and builds upon the lessons learned from the previous engine.

COMBUSTION, THERMODYNAMICS, AND SCALING

The rotary engine cycle can be described by either the Otto or Diesel cycle, depending on the ignition source (spark or compression ignition, respectively). The efficiency of both the Otto cycle engine and Diesel cycle engine is dependent on the compression ratio. As can be seen in Table 2, the compression ratio is dependent only upon the rotor generating radius (R) and the eccentricity (e) rather than the length scale of the engine. Therefore, decreasing the size of an engine does not affect the theoretical compression ratio or the theoretical thermal efficiency [9,10]

Otto Cycle: $$\eta_{th,Otto} = 1 - \frac{1}{r_v^{k-1}} \quad (1)$$

Diesel Cycle: $$\eta_{th,Diesel} = 1 - \frac{1}{r_v^{k-1}}\left[\frac{r_c^k - 1}{k(r_c - 1)}\right] \quad (2)$$

For the theoretical compression ratio of 19, the theoretical thermal efficiency of a spark ignited rotary engine (Otto Cycle) is 69%. For the same compression ratio, and assuming a cutoff ratio of 4:1 (typical for a diesel engine), the theoretical thermal efficiency of a compression ignited rotary engine (Diesel Cycle) is 56%. However, there are other factors that affect the design and efficiency of the engine due to the change from the macroscale to microscale. Issues include residence time vs. reaction time, increased heat loss, and quenching. Table 3 provides a qualitative review of the effect changing the length scale has on these issues.

Table 3. Effect of Decreasing Length Scale

Property	Effect	Comments
Residence Time	No change	Residence time ∝ 1/RPM
Chemical Rxn Time	No change	At same T
Quenching	Increases	Wall effect
Heat Loss Rate	Increases	Larger surface to volume ratio & wall effect
Thermal Stresses	Decreases	Due to uniform T

Residence time (swept time of rotor through combustion chamber) in a rotary engine is independent of size. Rather, the residence time is related to the operating speed of the engine. The power stroke of the rotary engine occurs over 90° of the rotor turn. At 40,000 RPM, the fuel / air mixture has 375 μsec to react before the exhaust port is uncovered. At normal combustion temperatures, hydrocarbons have a characteristic reaction time of 10 μsec [11]. Assuming $t_{res}/t_{chem} = 10$ for complete reaction, the maximum reaction time limited engine speed for a rotary engine is 150,000 RPM. Since the micro-rotary engine is designed to operate at an engine speed of 40,000 RPM, the reaction time is not a factor, if the temperature is kept elevated.

As the length scale of the engine decreases, the surface area to volume ratio increases as l^{-1}. A Biot number calculation [12]

$$Bi = \frac{hl}{k_{solid}} \quad (3)$$

$Bi = 3(10^{-4})$, assuming free convection and a conservative length scale of 2.5 mm for the engine block. This result suggests that the engine can be assumed to be operating with a uniform housing temperature distribution. The reduced temperature gradient between the hot (combustion / exhaust) and cold (intake) sides of the engine will reduce the effect of thermal expansion of the housing.

An isothermal housing implies that measures must be taken to control the amount of heat added to the incoming fuel / air mixture.

While pre-heating the intake fuel / air mixture will aid in obtaining combustion in the microscale, care must be taken to avoid autoignition in the inlet port. A further concern is that the heat added to the intake mixture will reduce the thermal efficiency due to the reduced T_H/T_C ratio of the cycle.

Flame quenching occurs due to cooling of the reaction, as well as radical destruction at the walls [13]. The minimum distance in the micro-rotary engine occurs at the point of maximum compression, when the fuel/air mixture is compressed between the rotor cutout and the side of the epitrochoid. The smallest linear distance of the micro-rotary engine is well below the quenching distance for any fuel. It has been determined that a flame can be stabilized in tubes well below the quenching diameter with an external heat supply to heat the tube wall [14]. In a supporting experiment, this strategy has been successfully employed using only the exhaust gas to heat the tube wall [15]. Based on these findings, the obvious solution to the quenching problem is to increase the temperature of the engine wall. The use of a SiC housing helps with this solution since there are no material constraints (SiC T_m = 3100°C). In fact, quenching can be totally eradicated if the wall temperature can be maintained at the adiabatic temperature of the fuel.

If thermal management is not sufficient to support gas phase combustion, the combustion reactions can be enhanced through catalytic surface reactions. It should be noted that for catalytic reactions, the increasing surface-area-to-volume ratio leads to overall higher conversion efficiency. For this purpose, the housing and rotor walls can be coated with a catalyst (e.g., Platinum).

From the point of view of combustion efficiency, the critical factor in MEMS combustion systems is the increased heat loss at small length scales. Heat loss decreases combustion temperatures, which leads to reduced reaction rate and quenching. Several strategies are being reviewed to reduce heat loss:

- Exhaust Gas Recirculation (EGR): A strategy that recirculates the combustion gases around the outside of the combustion chamber to decrease heat loss from the combustion chamber and pre-heat the incoming fuel-air mixture. The effectiveness of this strategy has been demonstrated [16]
- Stacking the engines to reduce the heat losses from the center engine(s). The center engine(s) will operate at nearly adiabatic conditions due to insulation and the higher melting temperatures of SiC
- An insulating channel filled with low conduction material, such as SiO_2, surrounding the engine

A significant problem facing large-scale rotary engines is leakage, either past the rotor tips or over the rotor face. Leakage reduces the engine efficiency (by reducing the compression ratio) and increases the effect of incomplete combustion. Sealing mechanisms have been created to reduce this problem in large-scale engines. These sealing systems consist of spring-loaded tabs at the rotor apexes [7] and across the rotor face. The tabs maintain contact between the rotor and epitrochoid walls and sealing for the chambers. Apex seals have been fabricated in the mini-engine, shown to be effective, and designed for the micro-rotary engine. A face seal system has not yet been developed that is compatible with MEMS fabrication. However, it should be noted that the smallest commercially available rotary engine (the 5000 mm^3 O. S. Graupner) does not use a face seal.

MINI-ROTARY ENGINE TEST BENCH

At the scale of the mini-rotary engine, there are no commercially available diagnostic engine test stands. Therefore, a test bench (Fig. 3) was designed and fabricated to test the mini-engine operation. The test bench consists of an electric motor / dynamometer, optical tachometer, ignition system (for spark plug use), and flywheel. A magnet on the flywheel is used to trigger the spark. Ignition and spark timing is achieved with a Hall Effect sensor mounted on a rotary dial and a spark ignition system manufactured by CH Electronics, Inc. Engine speed is measured using a Monarch Instruments ACT-3 tachometer with a ROS-5W remote optical sensor. The mini-engine is rigidly coupled to the dynamometer via a steel shaft.

To test combustion in the mini-rotary engine, a pre-mixed

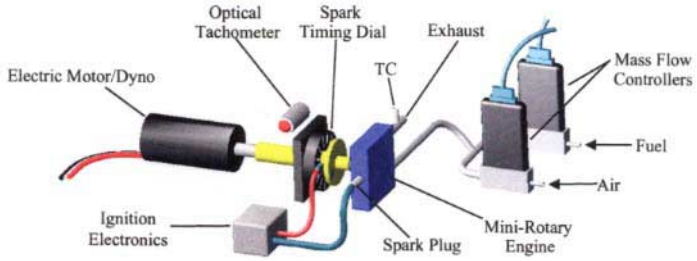

Figure 3. Mini-Rotary Engine Test Bench

hydrogen-air mixture is used rather than a liquid hydrocarbon, given hydrogen's ease of ignition. A gaseous fuel mixture is advantageous for this study because it does not require the complexity of a fuel carburetion system. The gaseous fuel and air are mixed upstream of the engine in a T-junction. The fuel is metered using valves and rotameters upstream of the T-junction.

To measure engine power, a dynamometer has been developed using a Maxon™ brushless electronically commutated motor and a rectifier circuit. Power generated by the mini-rotary engine spins the dynamometer, which acts as a generator and produces electrical power. The rectifier circuit converts the dynamometer's three-phase output to a DC voltage potential. Rheostats are used to apply a load to the dynamometer. The rheostats can be adjusted to produce the appropriate load, based on the mini-rotary engine being tested.

To calibrate the voltage across the dynamometer load to mechanical power output, the dynamometer is driven by an electric motor while connected to a torque arm and load cell. Figure 4 shows the calibration curve for the Maxon 50 W brushless DC motor.

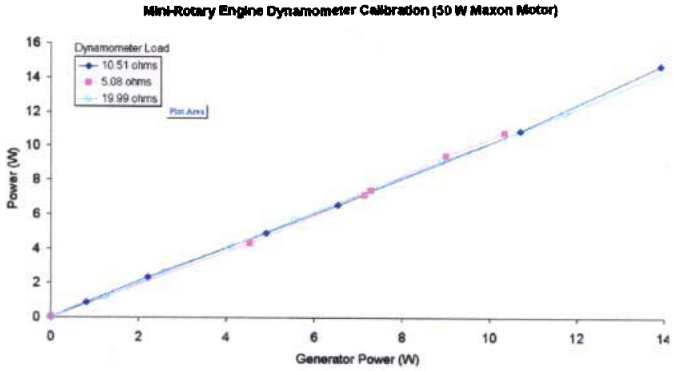

Figure 4. Dynamometer calibration chart for 50 W Maxon brushless electric motor.

Voltage drops across the rectifier circuit and across the engine coils were taken into account. During engine operation, the output voltage of the motor is measured and related to the power output through the calibration curve.

Temperature measurements were also made upstream of the engine and at the housing near the combustion chamber using thermocouple or infrared imaging. Pressure measurements upstream of the engine were also made to accurately measure fuel and air flow rates.

MN30 MINI-ROTARY ENGINE DESIGN AND TESTING

The MN30 generation mini-rotary engine is shown in Figure 5. The basic engine is simple in design, consisting of 7 parts: front plate, epitrochoid housing, back plate, rotor, internal gear, spur gear, and shaft. Two bearings, mounted in the front and back plate, position the shaft. For speed of fabrication, the mini-rotary engine is made from steel. The most accurate means of manufacture at this scale is through electrodischarge machining (EDM) [2]. Note that the initial design of the MN30 engine does not include apex or face seals.

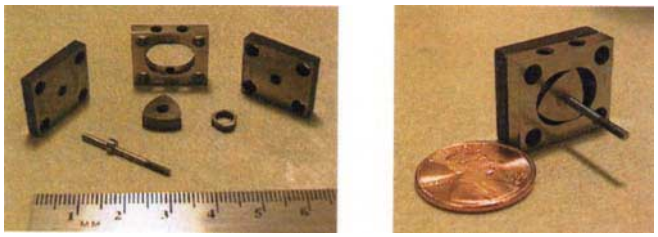

Figure 5. MN30 Mini-Rotary Engine

The MN30 mini-rotary engine has a displacement of 78 mm^3. Preliminary sealing tests determined that the engine suffered from 20% leakage during operation due to poor tolerances during manufacturing [17]. From the leakage tests, it was apparent that an apex sealing system was necessary. In order to improve sealing, slots were cut in the rotor apexes and apex seals inserted. The springs consist of brass tabs with leaf springs formed from spring steel (see Fig. 6). Even these simple designs significantly improved leakage.

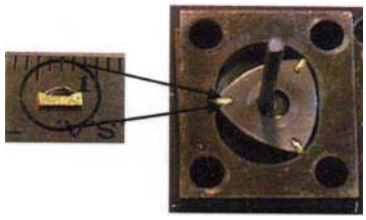

Figure 6. Modified MN30 Rotor with Apex Seals

Combustion tests were performed on the MN30 mini-engine with apex seals. In these tests, an electric motor was used to rotate the engine, while a stoichiometric H_2-air or H_2-C_3H_8-air mixture was supplied. The ignition system used was a spark plug. Ignition timing was changed from 15 degrees BTDC to 15 degrees ATDC. Figure 7 shows optical images of combustion obtained while operating the engine with a plexiglass front plate. While the engine generated no net power output, there was a 50% reduction in the power required by the electric motor to turn the mini-engine with combustion. Exhaust temperatures also changed with spark timing, with peak exhaust temperatures at 7.5 degrees BTDC.

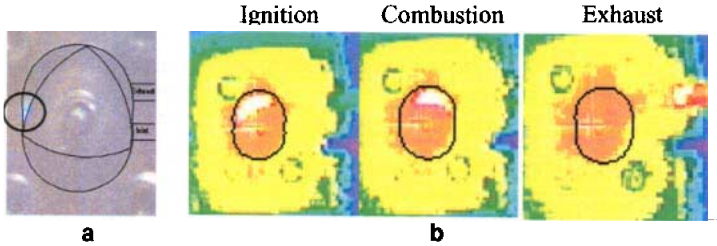

Figure 7. Optical Images of Ignition in MN30 mini-engine
a. High Speed Image of H_2-Oil-Air Ignition
b. Infrared Images of H_2-Air Ignition

MN125 MINI-ROTARY ENGINE DESIGN AND TESTING

Based on MN30 mini-engine testing, the following design features were incorporated into the MN125 mini-rotary engine:

- Integrated flexure apex seal system to test the applicability of the system in MEMS fabrication
- Exhaust gas recirculation to pre-heat the incoming fuel-air mixture and heat the combustion chamber with exhaust gases
- Increased size for better manufacturing tolerance

The displacement of the engine was increased from 78 mm^3 to 348 mm^3 to reduce the effects of manufacturing tolerance. The epitrochoid major and minor axes were increased by a factor of 1.33, while the width of the mini-engine was increased from 3.6 mm to 9 mm to reduce axial heat losses. The increase in width also allows for the use of commercial off the shelf (COTS) small-scale glow and spark plugs. Manufacturing tolerance of the MN125 engine was improved from ±0.2 mm to ±0.02 mm.

The MN125 engine generated positive output power operating on H_2-air and using two different ignition sources: 1) a COTS spark plug and 2) a COTS glow plug. The experimental results of tests with the spark ignition will be discussed first. The test procedure typically consists of the following: the MN125 is initially brought up to speed through the use of pressurized air to overcome friction. The spark system is energized and H_2 introduced into the flow until sustained combustion is obtained. The power generated by combustion results in an increase in engine speed and voltage across the dynamometer load. When the spark is energized, the voltage across the dynamometer load, engine speed, and housing temperature all increase.

During the experiment shown in Figure 8, the spark is turned off at three separate times for 5-10 seconds to achieve steady,

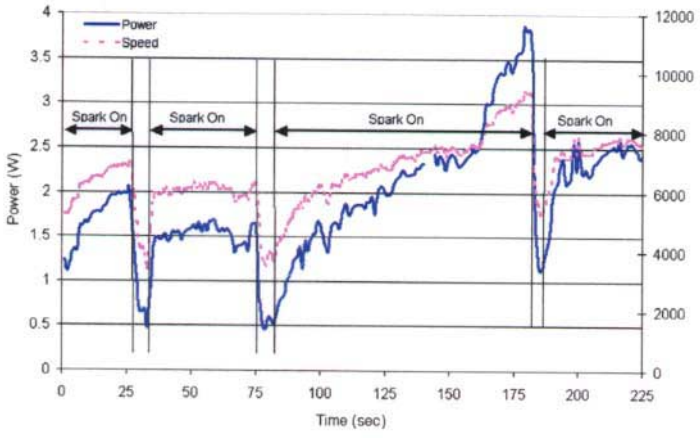

Figure 8. Engine power output and engine speed of a MN125 mini-rotary engine operating on H_2-air using a spark ignition.

non-combustion conditions. Without combustion, there is a decrease in engine speed, measured power, and a 1°C/sec decrease in housing temperature due to heat loss to the engine stand and convection.

This difference in power output immediately before the spark is terminated and after the engine reaches a steady state without combustion (spark off) is the net power output of the MN125 mini-engine. Figure 8 shows a plot of engine power and engine speed. For this particular experiment, the net power output at 25 and 75 seconds is 1.5 W and 1.2 W, respectively. The stoichiometry during this time period is Φ=0.42. At 100 seconds, air flow is increased to measure power output at higher engine speeds. This leads to an increase in engine power output to 2.7 W with a stoichiometry of Φ=0.37 due to the increased air flow rate. Spark timing for all three power measurements is 0 degrees BTDC.

Equivalence ratios closer to stoichiometric will give higher power, but flashback (related to leakage) prevents the experiment from reaching higher equivalence ratios. The experiment was terminated because of lubrication breakdown due to elevated engine temperature. In a separate test, the breakdown temperature of the lubricant was measured to be $T_{breakdown}$ = 275°C.

The net power output as a function of the peak engine speed for a MN125 mini-engine is compiled in Figure 9. The plot indicates a linear rise in power with engine speed consistent with a relatively constant torque output. This indicates the residence time is greater than the reaction time. The scatter in the data is due to slightly different operating conditions during each test. Stoichiometries for these tests vary between Φ= 0.4 ± 0.04, while the spark timing is maintained at 0 degrees BTDC. The maximum power obtained by the engine is 2.7 W at 9300 RPM with η_{th} of less than 0.5%. It should be noted that this is the result of preliminary tests of the MN125 engine. Further tests will incorporate thermal management, improved sealing, and optimized inlet / exhaust ports.

Tests have begun using an O.S. Engines Type RE glow plug as the ignition source. Initial tests with H_2-air have also shown positive power generation. The glow plug uses platinum or a platinum-composite for the heater coil. Since the platinum acts as a catalyst during engine operation, power is only needed to start the engine. This result is critical for implementation in the micro-rotary engine, as a spark ignition system would require too much energy for a MEMS system.

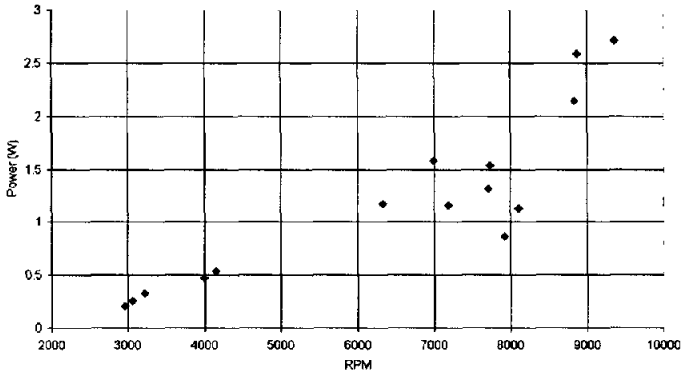

Figure 9. Net power output of Gen II mini-rotary engine operating on H_2-air and using spark ignition (Φ = 0.4 ± 0.04)

MN50 MINI-ROTARY ENGINE DESIGN AND TESTING

The MN50 mini-rotary engine has been designed and fabricated for operation with liquid fuel (Fig. 10). This engine has a displacement of 138 mm^3. Design features of the MN50 include a new rotor profile for improved sealing and compression and a liquid fuel carburetor.

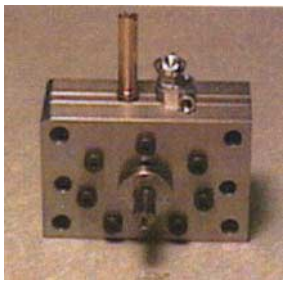

Figure 10. MN50 Mini-Rotary Engine with Liquid Fuel Carburetor

Engine temperature affects lubrication and performance of the engine. As engine temperature increases, engine lubricants break down, which leads to increased leakage across the apex seals and reduced compression ratio. The use of a liquid fuel with incorporated lubricant is necessary.

Initial testing of the MN50 mini-rotary engine using H_2-air has commenced. Positive power output of the MN50 engine operating on H_2-air has been observed. When the spark is turned on and off, the engine speed responds accordingly. Testing of the MN50 mini-engine with liquid hydrocarbon (Methanol-Nitromethane) fuels will follow.

MEMS-ROTARY ENGINE FABRICATION

Design and fabrication of the MEMS-scale rotary engine (micro-rotary engine) has begun. A larger scale "meso-rotary" engine was fabricated at the Case Western Reserve University (CWRU) MEMS Research Center using Si and SiC. The CWRU micro-engine has a displacement of 1.2 mm^3 and a rotor diameter of 3 mm, compared to the ultimate goal of 0.08 mm^3 displacement and 1 mm rotor diameter. The larger engine was fabricated to test the limits of the CWRU SiC fabrication process.

The rotor is made of molded SiC [18] from a three-wafer Si mold (see Fig. 11). The Si housing is fabricated from three separate 500 mm wafers deep reactive ion etched (DRIE) to form the features and then fusion bonded together (see Fig. 12).

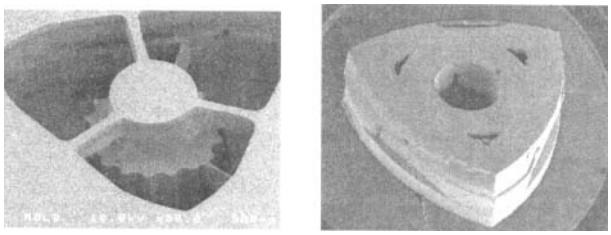

Figure 11. CWRU Micro-Rotary Engine Left: Three-wafer Si mold Right: Molded SiC rotor

The CWRU micro-engine highlights some of the difficulties in fabricating an engine using MEMS techniques. Even though the tolerance obtained in MEMS is typically on the order of microns, the percentage tolerance when compared to the length scale is high. For a high precision system such as the rotary engine, the tolerance required is on the order of 0.1% (<1μm). This tolerance is complicated by potential misalignments of the three-layer Si mold when fusion bonded together. A ridge can be seen on the SiC rotor in Figure 11, as well as

one in Figure 12 for the Si housing due to a 20 μm misalignment. Work on the next generation CWRU meso-engine has begun with the aim of higher manufacturing tolerances.

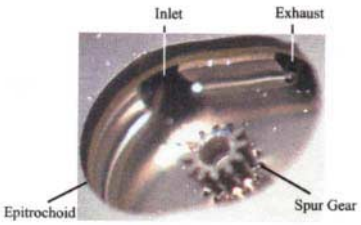

Figure 12. CWRU Micro-Rotary Engine Housing

Fabrication of the 1 mm diameter micro-rotary engine has commenced. The micro-rotary engine will be fabricated using bulk Si etching techniques at the U.C. Berkeley Microlab with a SiC thin coating for protection against high stresses, temperatures, and chemicals [6].

CONCLUSION

Power MEMS is an emerging field that may ultimately produce portable power generation systems with an order of magnitude higher energy density than common batteries. The combination of low unit cost through mass production and high energy density through liquid hydrocarbon fuels shows great promise.

A research project has begun with the objective to design, fabricate, and obtain positive power output from a micro-rotary internal combustion engine. A series of mini-rotary engines have been manufactured and tested to investigate the effect of scale reduction on sealing, fluid, and combustion issues. The mini-rotary engines have been operated on gaseous H_2-air using both spark and glow plugs as the ignition system. Positive power output of up to 2.7 W at ~9,300 RPM has been obtained from the MN125 mini-rotary engine. Further refinement of the mini-engine is necessary to increase engine efficiency through improved sealing and thermal management. Engine operation is affected by engine temperature and fuel-air stoichiometry. Richer mixtures are necessary for improved power output. However, thermal management schemes are necessary to prevent pre-ignition in the inlet port. The results obtained to date with small-scale engines indicate that there are no fundamental phenomena that would prevent the development of the micro-rotary engine.

Fabrication of the micro-rotary engine has begun with a larger scale meso-engine fabricated at Case Western Reserve University. The challenges facing the fabrication of the micro-rotary engine include manufacturing tolerances, wafer alignment, assembly, and materials. Fabrication of the micro-rotary engine has begun at U.C. Berkeley.

ACKNOWLEDGEMENTS

This work is supported by DARPA through Grant Number DABT63-98-1-0016. The authors would like to thank Professor Mehran Mehregany and Dr. Chris Zorman of the MEMS Research Center at Case Western Reserve University and Ms. Miki Yamada of the University of California at Berkeley. The authors would also like to thank Maroney Company for their assistance in the fabrication of the mini-rotary engines.

REFERENCES

1. Kovacs, G. T. A., 1998, *Micromachined Transducers Sourcebook*, Mc-Graw-Hill, New York.
2. Madou, M., 1997, *Fundamentals of Microfabrication*, CRC Press, Boca Raton.
3. Waitz, I.A., Gauba,, G., Tzeng, Y-S., 1996, "Combustors for Micro-Gas Turbine Engines", Proceedings of the ASME Aerospace Division.
4. Linden, D., 1995, *Handbook of Batteries 2nd ed.*, McGraw-Hill, New York.
5. Mehregany, M., Zorman, C. A., 1999, "SiC MEMS: Opportunities and Challenges for Applications in Harsh Environments", Thin Solid Films, **355-356**, pp. 518-524.
6. Stoldt, C. R., Carraro, C., Ashurst, W. R., Fritz, M. C., Gao, D., Maboudian, R., 2001, "Novel Low-Temperature CVD Process for Silicon Carbide MEMS", Proceedings, accepted to Transducers 2001, International Solid-State Sensors and Actuators Conference.
7. Norbye, J.P., 1971, *The Wankel Engine: Design, Development, Applications*, Chilton Book Co.
8. Ansdale, R.F., Lockley, D.J., 1969, *The Wankel RC Engine*, A.S. Barnes and Company, South Brunswick.
9. Van Wylen, G. J., Sonntag, R. E., 1986, *Fundamentals of Classical Thermodynamics, 3rd ed.*, John Wiley and Sons, New York.
10. Cengel, Y. A., Boles, M. A., 1994, *Thermodynamics, An Engineering Approach*, McGraw-Hill, New York.
11. Borman, G. L., Ragland, K. W., 1998, *Combustion Engineering*, McGraw-Hill, Boston.
12. Incropera, F., DeWitt, D., 1996, *Fundamentals of Heat and Mass Transfer*, John Wiley & Sons, New York.
13. Glassman, I., 1996, *Combustion, 3rd ed.*, Academic Press, San Diego.
14. Zamashchikov, V. V., 1997, "Experimental Investigation of Gas Combustion Regimes in Narrow Tubes", Combustion and Flame, **108**, pp. 357-359.
15. Fu, K., Knobloch, A. J., Cooley, B. A., Walther, D. C., Fernandez-Pello, C., Liepmann, D., Miyasaka, K., 2001, "Microscale Combustion Research for Applications to MEMS Rotary IC Engine", Proceedings, accepted to 2001 National Heat Transfer Conference.
16. Cooley, B., 1999, ," Exploring the Limits of Microscale Combustion" Master's thesis, University of California, Berkeley, CA.
17. Fu, K., Walther, D. C., Fernandez-Pello, A. C., Liepmann, D. and Miyasaka, K., 1999, "Preliminary Report on MEMS Rotary Internal Combustion Engine", Proceedings, Western States Section Fall Meeting.
18. Rajan, N.; Mehregany, M.; Zorman, C. A.; Stefanescu, S.; Kicher, T. P., 1999, "Fabrication and Testing of Micromachined Silicon Carbide and Nickel Fuel Atomizers for Gas Turbine Engines", Journal of MicroElectroMechanical Systems, **8**, No. 3, pp. 251-257.